Journal of Nuclear Materials 408 (2011) 183–187

Contents lists available at ScienceDirect

Journal of Nuclear Materials

journal homepage: www.elsevier.com/locate/jnucmat

Surface segregation and adsorption effects of iron–technetium alloys from first-principles

Christopher D. Taylor *

Materials Technology – Metallurgy, Materials Science Division, Los Alamos National Laboratory, Los Alamos, NM 87545, United States

ARTICLE INFO

Article history:
Received 5 August 2010
Accepted 16 November 2010

ABSTRACT

Surface properties of Tc-rich and Fe-rich portions of the Tc–Fe binary alloy phase diagram were computed in this work on the basis of density functional theory. Tc and Fe were found to have minimal degrees of mixing in the parent phases, consistent with the experimentally derived phase diagram. The influence of oxygen on surface phase stability was also studied, with no significant impact on surface segregation or degree of surface mixing. Oxygen adsorption was shown to change the ordering of surface facets in Tc, such that the pyramidal phase becomes lower in energy than the prismatic phase, even with low coverage of oxygen. No evidence for increased surface segregation upon oxidation was found for the solid-solution phases. A potential–pH surface Pourbaix diagram was derived for Tc and H, OH and O adsorbed sub-monolayers were shown to be precursors to oxide formation. While Tc and Fe have similar reactivities and properties in their parent phases, and hence, also in solid-solution, the properties of the intermetallic are expected to be significantly different due to the size-mismatch between the elements.

1. Introduction

A fundamental understanding of the reactivity and corrosivity of waste forms containing metallic Tc and alloys properly begins with the underlying properties of the metallic surfaces themselves. As a transition metal, Tc is expected to have oxide forming properties that may provide some form of passivity depending on the local conditions of pH and electrochemical potential [1]. At the same time, the difficulties associated with handling Tc have hindered the same degree of corrosion, surface science and electrochemical investigation that has benefited the utilization of other transition metals. While a handful of studies have been published describing the ab initio computation of some fundamental materials properties of Tc [2–5], none have focused on the materials/environment interface; and, at present, few surface measurements have been performed on clean, well-characterized Tc or Tc-alloy surfaces [6]. To expand upon the current state of knowledge of materials and surface properties of these alloys, we have begun to develop a program of combined atomistic modeling techniques and high-resolution surface science probes to begin to characterize the fundamental properties of Tc-alloy surfaces, beginning with bare metallic surfaces exposed to ultra-high vacuum (UHV) conditions, and moving up to more complex models and experimental setups that approach anticipated storage scenarios. This work builds on the foundations of previous ab initio and experimental corrosion studies [7–9]. In the present work we describe the initial ab initio calculations for Tc and Fe metallic slabs, created to model exposed low-index surface facets of these metals, the Tc–Fe intermixing properties expected for these slabs at the extreme ends of the binary phase diagram [10] relative to their mutual bulk solubilities, and the reactivity of these surfaces towards both atmospheric oxygen and aqueous environments. This research provides the foundation for future atomistic studies of the oxidation and corrosion of this binary alloy system, as well as for studies of ternary systems, including Mo, for example. The approach follows that of previous computational studies of corrosion properties of metal surfaces [11,12].

2. Computational details

The ab initio calculations of surface energies and reactivities were performed according to the formulations of density functional theory [13], in which the electron density is iteratively computed from the Kohn–Sham equations [14]. The PBE functional was used to model the unknown exchange–correlation component of the total energy functional [15]. The Vienna Ab initio Simulation Package (VASP) was utilized to solve the relevant equations and optimize the system geometries [16]. The Kohn–Sham orbitals were expanded into a plane-wave basis of up to 400 eV, and the method of projector-augmented waves (PAW) was selected [17]. The computations for Fe provide bond-lengths and surface energies in good agreement with previous results, [18] and, similarly, for the known properties of Tc [2]. We therefore proceeded to apply this methodology with good confidence for the elucidation of the unknown quantities being sought in this work. The method

* Tel.: +1 505 667 5499.
E-mail address: cdtaylor@lanl.gov

0022-3115/$ - see front matter © 2010 Elsevier B.V. All rights reserved.
doi:10.1016/j.jnucmat.2010.11.032

of computation of other parameters (surface energies, adsorption energies) will be described as they are introduced in the following section.

3. Results and discussion

3.1. Surface energies and work functions of Tc and Fe low-index surfaces

Surface energies were determined for the low-index surfaces of Fe and Tc considered herein using the formula:

$$\gamma = E[\text{slab}] - N_{\text{slab}}E[\text{bulk}]/2A[\text{slab}] \quad (1)$$

where E[slab] is the energy of the slab model of the surface obtained from density functional theory, E[bulk] is the energy per atom in the parent bulk structure obtained from density functional theory, N_{slab} is the number of atoms in the slab model, and A[slab] is the slab area. The factor of two arises from the exposure of two surfaces per slab model due to the periodic boundary conditions employed.

Work functions were determined by plotting the average electrostatic potential in the slab supercell as projected in the direction normal to the slab surface. The electrostatic potential in the vacuum is set as 0 V, and the Fermi potential of the system corrected accordingly, thus producing the work function.

The surface energies and work functions calculated using density functional theory for Fe(1 0 0), Fe(1 1 0) and Fe(1 1 1) are consistent with those reported previously [18] (Table 1). When compared to Tc(0 0 0 1), Tc(1 0 −1 0) – the prismatic plane – and Tc(1 0 1 1) – the pyramidal plane (Fig. 1), we find that the values for both work functions and surface energies are quite similar between the two metals. The work function ranges between 3.91 and 4.76 for the various low-index surfaces of Fe, and between 4.19 and 4.66 for the low-index surfaces of Tc. We note that the computed work function for Tc(0 0 0 1) is compatible with the work functions reported for the surrounding elements in the periodic table. Likewise, the surface energies range from 2.43 through 2.68 J/m^2 for Fe and from 2.37 through 2.71 J/m^2 for Tc. The lowest energy surface facets are the (1 1 0) plane for Fe, and the (0 0 0 1) basal plane for Tc metal.

The similarities between the surface properties of Tc and Fe imply that neither Fe nor Tc would preferentially segregate to the surface in any alloy scenario; and that both metal surfaces would likely react equally well with oxidants in the environment. This behavior is rather ideal in that we would anticipate that Tc would not act as a cathodic source, catalyzing the dissolution of Fe from the alloy, neither would Fe act in a converse manner for Tc. In future work we will also examine the predicted surface structure of the FeTc σ-phase intermetallic compounds. Direct calculation and comparison of reactivities with oxygen will be presented in a following section, and corrosion scenarios (such as surface vacancy formation via dissolution) will be examined in future work.

Since the (1 1 0) facet of Fe and the basal (0 0 0 1) facet of Tc are anticipated to be the most prevalent on exposed surfaces of these metals, we will focus predominantly on these surface planes in the following mixing and oxygen adsorption studies.

Table 1
Surface energies and work functions calculated for Fe and Tc low-index planes.

Surface	Work function (eV)	Surface energy (J/m^2)
Fe(1 0 0)	3.91[a] 3.98 (this work)	2.68 (2.47[a])
Fe(1 1 0)	4.76[a] 4.78 (this work)	2.43 (2.37[a])
Fe(1 1 1)	3.95[a] 3.90 (this work)	2.59 (2.54[a])
Tc(0 0 0 1) *basal*	4.66	2.37
Tc(1 0 −1 0) *prismatic*	4.48	2.61
Tc(1 0 −1 0) *pyramidal*	4.19	2.71

[a] Results from Blonski and Kiejna [18].

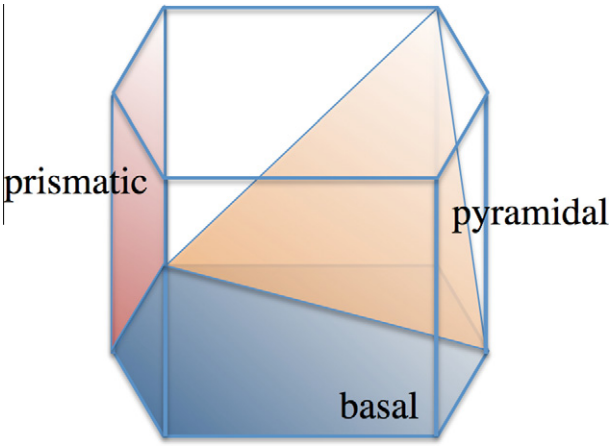

Fig. 1. Low-index planes in hcp metals. Basal (0 0 0 1), prismatic (1 0 −1 0) and pyramidal (1 0 1 1).

3.2. Mixing properties of bulk and surface Tc–Fe binary systems

The preferential segregation of one component of an alloy to the surface can significantly affect the corrosion properties of the alloy. By performing calculations of the relative mixing energies for each alloy component in the bulk versus the surface environment the segregation properties can be elucidated. A series of supercell and slab models were constructed to examine these properties for the Tc–Fe binary system. First, a body-centered-cubic supercell consisting of 128 Fe atoms was constructed, and the energy associated with replacing one Fe atom by Tc was evaluated, using the equation below:

$$E_{\text{mix}}(\text{Tc}|\text{Fe}) = E(\text{Fe}_{127}\text{Tc}) - 127 * E(\text{Fe}|\text{Fe}) + E(\text{Tc}|\text{Tc}) \quad (2)$$

where $E(\text{Fe}_{127}\text{Tc})$ is the energy of the modified Fe supercell containing Tc, E(Fe|Fe) is the energy of Fe in the bulk system per Fe atom, and similarly for E(Tc|Tc). The value computed for E_{mix}(Tc|Fe) is therefore the energy cost to the entire system resulting from the displacement of an Fe atom by Tc. A mixing energy of +0.15 eV/Tc atom was obtained from this equation, relative to the Tc hexagonal close packed state.

In order to understand the opposite behavior, that is, the properties of Fe dissolved in Tc, an Fe atom was placed in a 96 atom Tc hexagonal closest packed supercell. A comparable energy of 0.15 eV/Fe atom was obtained in this second case. There is therefore a mildly endothermic enthalpy of dissolution for Fe in Tc and Tc in Fe, respectively. Applied to a simple Boltzmann distribution, these results imply mutual solubilities of Fe in Tc and Tc in Fe of 0.2 atomic% at 300 K. This number is consistent with the vanishing solubilities observed at either end of the experimentally derived phase diagram for temperatures below 900 °C [10]. To our knowledge exact measurements of the terminal solubilities have not been made.

The production of intermetallic phases with differing crystallographies and potentially greater levels of intermixing between Tc and Fe, such as the sigma phase observed between Tc compositions of 40% and 65% by Darby et al. [19] will be considered in future work.

To investigate surface segregation effects we prepared two slab systems – five layer Tc(0 0 0 1) and Fe(1 1 0) low-index planes – and apply various substitutions. These included replacing a surface layer atom with one of the opposite species, doing this for the

sub-surface and sub-sub-surface layers, and finally replacing the entire surface layer with a 'skin' of the opposite species. The coverage replacement by the minority atom was at the level of one atom per nine in the total layer, or 0.11 ml. The segregation energies can then be obtained by comparing each of these slab energies, with the energies of the pristine slabs, assuming that the displaced atoms relocate back into the bulk and the introduced atoms originated in the bulk. i.e. the segregation energies are given by the equation:

$$E_{\mathrm{mix}}(\mathrm{surf}) = [E(\mathrm{A_xB_y}) - E(\mathrm{A}_x + y) - yE(\mathrm{B|B}) + yE(\mathrm{A|A})]/y \quad (3)$$

$E(\mathrm{A_xB_y})$ is the energy of the slab model where y atoms of B is embedded in the slab consisting of x atoms of A. $E(\mathrm{A}_{x+y})$ is the energy of the slab model consisting purely of species A. E(B|B) is the energy of species B embedded in its own host matrix, similarly for E(A|A), and E_{mix}(B|A) is the enthalpy for mixing species B into the bulk of species A, as described above. Using this equation a segregation energy of zero would imply that there is no preference for either the bulk or the surface of the system. Positive segregation energies would imply a preference for the bulk, and negative segregation energies a preference for the surface.

In the case of Fe(1 1 0), therefore, four cases were considered: replacing a surface atom with Tc, a sub-surface atom, and a sub-sub-surface atom, as well, as substituting the entire surface skin. The segregation energies for each of these cases were determined to be 0.07 eV, 0.05 eV, −0.08 eV, and 0.19 eV (skin), respectively (Table 2). These slight energies suggest that there is no strong preference between the bulk or the surface for Tc atoms when embedded in a body-centered-cubic iron matrix, at least on the (1 1 0) surface. In all cases it is implied that Tc prefers the interior of the Fe parent lattice compared to being embedded in the most compact Fe(1 1 0) surface. The epitaxial skin state for Tc over Fe(1 1 0) is disfavored relative to bulk dissolution by 0.19 eV per Tc atom.

In the case of Fe interacting with Tc(0 0 0 1), very similar behavior emerges from the computed results. This observation is consistent with the already noted similarity between the Tc and Fe surface energies and work functions. In a Tc host, the segregation energies for iron in the surface, sub-surface, sub-sub-surface and skin scenarios are 0.02, 0.03, −0.1 and 0.13 eV, implying that Fe does not preferentially integrate as a surface species on Tc(0 0 0 1). Furthermore, direct epitaxial skin layers of Fe over Tc(0 0 0 1) are not energetically favorable (Table 2).

These results taken together imply the following:

(1) Fe and Tc have weak mixing tendencies; with predicted mutual solubilities of 0.2 atomic% at 300 K.
(2) This weak mixing extends to the surface case, where one may have predicted that the additional degree of freedom could have provided some opportunities for the crystal structures to relax. It is possible that the formation of novel surface states, not considered in this work, may alleviate some of the strains resulting from the size-mismatch between these atoms (r_{Fe} = 0.245 nm < r_{Tc} = 0.272 nm). Such structures will be investigated in future work using molecular dynamics, and modified embedded atom simulations. The fact that impurity embedding was found to be endothermic in the lowest energy surfaces, may be a consequence of the higher degree of compactness of these surfaces compared to the higher energy surface planes.
(3) Investigation of both bulk and surface properties of Fe–Tc intermetallic phases should be pursued. One candidate to particularly focus on is the disordered sigma phase produced by Darby at Tc compositions around 50% [19].

Table 2
Segregation energies for Tc in Fe(1 1 0) and Fe in Tc(0 0 0 1) for surface, sub-surface, sub-sub-surface and skin residence scenarios.

Model	Surface	Sub-surface	Sub-sub-surface	Skin
Tc in Fe(1 1 0)	0.07	0.05	−0.08	0.19
Fe in Tc(0 0 0 1)	0.02	0.03	−0.1	0.13

3.3. Oxygen adsorption on Tc–Fe surfaces

The surface properties reported above apply strictly to an UHV environment. Exposure to an oxidizing environment could potentially modify the emergence of these phases, including changes to the energetically preferred surface facets and segregation tendencies. By computing the adsorption energy for oxygen on these surfaces, relative to the O_2 molecular state, we can provide a measure for how much the surface will be stabilized by reaction with oxygen. These oxygen adsorption energies are tabulated for the various surfaces in Table 3.

The oxygen adsorption energies are computed here to vary widely depending on the surface plane used. This is the case for both Tc and Fe. The results for Fe are in good agreement with those obtained by Blonski et al. [20]. The strongest adsorption energies for Tc and Fe are, once again, comparable in strength (−3.75 for Fe(1 1 0) compared to −3.67 for Tc(0 0 0 1)). Thus Tc and Fe are predicted both from work function, surface energy, and adsorption energies to have comparable surface reactivities. Although an Fe skin on Tc(0 0 0 1) does not significantly impact the adsorption energy, a Tc skin on Fe(1 1 0) does raise the adsorption energy by 0.4 eV (Table 3). As the oxygen adsorption energy is not stronger for any of the surface segregated phases, compared to the parent phases, it is not expected that oxygen will promote surface segregation in Fe–Tc alloys.

Surface energies may be computed as a function of oxygen coverage using the equation:

$$E[\mathrm{surf}] = \gamma + \theta * E_{\mathrm{ads}}(\mathrm{O})/A \quad (4)$$

θ, the coverage of oxygen, modifies the surface energy by an amount equivalent to the fractional area multiplied by the adsorption energy, scaled by the area per metal atom, A. The coverage of O can be related to either a chemical potential for O, provided from the atmosphere, for example, or to an electrochemical source such as the decomposition of H_2O or OH^-. As the oxygen adsorption energies are in general quite exothermic, very little oxygen over-pressure would be required to induce oxide formation on the surface through this surface adsorption mechanism. Under aqueous conditions the pH and local electrochemical potential will play an important role (see next section).

When the surface energy is plotted against the oxygen coverage, under the assumption that the oxygen adsorption energies will remain constant with increasing coverage (as the coverage increases beyond 0.5 ml this is unlikely to hold true due to lateral interactions between the adsorbates), we find that the ordering of the energies of the Tc surface facets changes (Fig. 2). The

Table 3
Oxygen adsorption energies on facets of Tc and Fe as well as mixed surface phases. Oxygen adsorption energies include the zero-point energy of O_2. Adsorption energies for the low-index planes were computed at 0.25 ml O coverage. Surface-substituted systems were computed at 0.11 ml O coverage.

Surface	E_{ads}(O) (eV)	Surface	E_{ads}(O) (eV)
Fe(1 0 0)	−3.75	Tc(0 0 0 1) *basal*	−3.67
Fe(1 1 0)	−3.47	Tc(1 0 −1 0) *prismatic*	−3.47
Fe(1 1 1)	−2.54	Tc(1 0 −1 1) *pyramidal*	−3.48
Fe(1 1 0)–Tc$^{(\mathrm{surf})}$	−3.35	Tc(0 0 0 1)–Fe$^{(\mathrm{surf})}$	−3.62

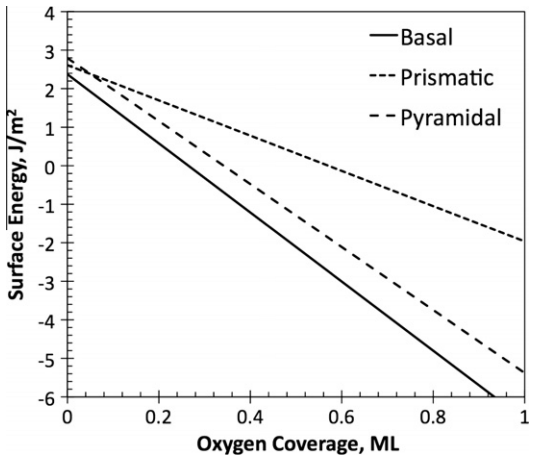

Fig. 2. Tc low-index plane surface energies in the presence of adsorbed oxygen.

pyramidal plane has a stronger oxygen adsorption energy than the prismatic plane, which makes it overall lower in energy than the prismatic plane at coverages <0.04 ml of oxygen. Due to the rather strong binding energy of oxygen to the Tc surfaces, the surface formation energy can even become negative, at which point oxide formation is expected to occur and the metallic phase itself will become inherently unstable. The results of Fig. 2 imply that adsorption of oxygen on the basal plane at around 0.25 ml will result in a strong destabilization of the Tc metal itself (i.e. surface energies become negative), implying that oxide formation will become dominant under these conditions. The curves are expected to take a position deviation from linearity around 0.5 ml. The range between 0.1 and 0.3 ml should be reliable as oxygen adsorption energies were explicitly computed within this range.

3.4. Electrochemical processes at the Tc|H_2O interface

A second model based on water as the oxidizing source can also be constructed. In this case we consider the free energy associated with the reaction:

$$M + H_2O \rightarrow M{-}O(ads) + 2H^+ + 2e^- \quad (5)$$

When we computed the direct adsorption of water on Tc(0 0 0 1), the water molecule directly dissociated to form OH and H on the surface. We therefore also consider the reactions:

$$M + H_2O \rightarrow M{-}OH(ads) + H^+ + e^- \quad (6)$$

$$M + H^+ + e^- \rightarrow M{-}H(ads) \quad (7)$$

There will be an equilibrium potential, U_{eq}, associated with all of these processes, that we can determine by considering the free energies of the reactions and applying the Gibbs' equation. To simplify the determination of the electrochemical potential, we will take advantage of the equality $G[H_2] = 2G[H^+]$ when the electrochemical potential is 0 V NHE (normal hydrogen electrode) [21]. Hence:

$$U^{eq}[O] = (E[M{-}O] - E[M] - E[H_2O] - \Delta G[H_2O]_T + E[H_2] + \Delta G[H_2]_T - 2 * 2.303\ kT\ pH)/2 \quad (8)$$

$$U^{eq}[OH] = E[M{-}OH] - E[M] - E[H_2O] - \Delta G[H_2O]_T + 1/2\ E[H_2] + 1/2\ \Delta G[H_2]_T - 2.303\ kT\ pH \quad (9)$$

$$U^{eq}[H] = -(E[M{-}H] - E[M] - 1/2\ E[H_2] + 1/2\ \Delta G[H_2]_T + 2.303\ kT\ pH) \quad (10)$$

A value of 0 V for U^{eq} would imply that the reaction is thermoequivalent to the H_2/H^+ equilibrium. Changes in U^{eq} due to changes in the pH are introduced by the 2.303 kT pH term, which moves the chemical potential for hydrogen up or down, accordingly. The ΔG terms are applied to augment the theoretical energies with computational or experimental specific heat capacities, and zero-point energy terms. These can be derived from the JANAF tables and other resources [22,23]. For H_2O we derive the value 0.57 eV based on the free energy of H_2O relative to an isolated molecule at 0 K. The zero-point energy from the Computational Chemistry Comparison and Benchmarking Data Base is 0.59 eV. For H_2 we have a ΔG value of 0.31 eV, and a zero-point energy of 0.27 eV. The factor of 2 in the equation for $U^{eq}[O]$ comes from the fact that the oxidation process here is a 2-electron reaction.

The free energies so determined are plotted for the scenario pH = 0 in Fig. 3. This figure shows that exposed Tc(0 0 0 1) facets will encounter three regions of stability: Tc–H(ads), Tc–OH(ads) and Tc–O(ads), depending on the electrochemical potential. This trend has been observed for other transition metals, both experimentally [24–26], and via theoretical analysis [12,27].

By plotting numerous such diagrams at various pH conditions, or, alternatively, solving for the intersection points as shown in Fig. 3 algebraically, a predominance diagram can be plotted for the Tc(0 0 0 1) surface. In electrochemistry, predominance diagrams can be used to predict which phases will be present as a function of potential and pH. Other variables sometimes considered are temperature and the concentrations of other species that may be present in the environment [1]. By solving for the equilibrium conditions existing between Tc–H(ads) and Tc–OH(ads), as well as Tc–OH(ads) and Tc–O(ads) it is possible to construct the predominance diagram shown in Fig. 4. In order to understand how the surface phases interact with the bulk oxide phases, the bulk Pourbaix diagram for Tc has been superposed upon the computed surface information.

It can be seen from Fig. 4 that activation of water chemistry occurs prior to TcO_2 formation. Hence, a surface film of oxygen will form on technetium prior to formation of the bulk oxide as the pH is increased or the potential is raised. This behavior is different to that of Cu, in which a hydroxide film was observed to be the immediate precursor to oxide formation [24]. There are also regions in the predominance diagram in which OH and H films are predicted to be stable on the Tc surface. Verification of these predictions could potentially be made using high-resolution microscopy or spectroscopic techniques.

The 'pre-passive' process of OH and O film formation on metal surfaces has been proposed as an important step in the development of metal passivity [24]. Furthermore, the interruption of

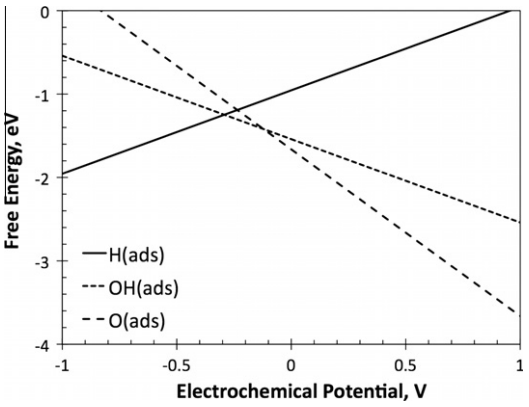

Fig. 3. Free energy of the adsorption reaction for H(ads), OH(ads), and O(ads) plotted for a pH of 0 at 300 K.

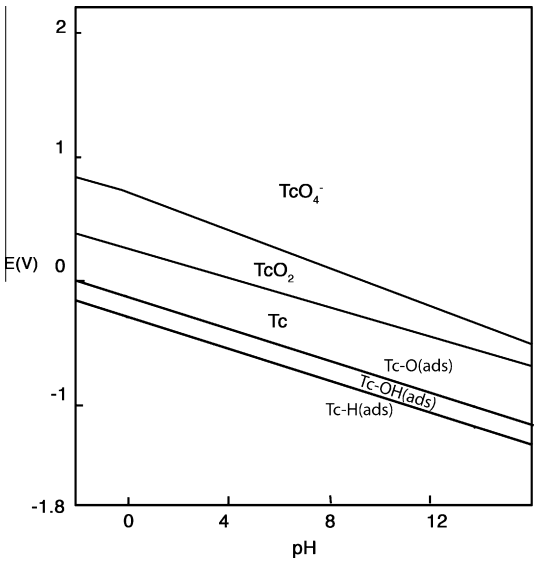

Fig. 4. Potential-pH diagram illustrating regions of Tc stability regarding the water dissociation and hydrogen adsorption reaction, based upon the free energy diagrams in Fig. 3. The surface adsorption regions are superposed upon the bulk phases obtained from Pourbaix [1].

these processes, via competitive surface adsorption, for example, has been suggested as one mechanism via which environmental contaminants may hinder repassivation of damaged metal surfaces, thereby leading to localized corrosion events [28]. As development of metal waste forms containing Tc progresses, the consideration of such ageing and leaching mechanisms may become of greater significance.

4. Conclusions

The overall picture emerging from this work is that Tc and Fe are expected to have very similar surface properties. Despite this, the elements have an endothermic enthalpy of mixing, which leads to expected mutual solubilities of around 0.2%, consistent with the known binary phase diagram. Furthermore, the alloy surface properties at either extreme end (low Fe content, or low Tc content) are expected to be dominated by the majority element: There is no evidence for surface segregation of the minority species. Even should there be surface segregation, as directly tested herein, the surface properties of Tc and Fe are rather similar in terms of surface energy, work function, and oxygen dissociative adsorption. For both Tc and Fe there is a strong exothermic tendency to dissociate oxygen on the surface, and this effect lowers the surface energy of the metals. Consideration of the electrochemical activation of water on Tc indicates that oxide formation will be preceded by sub-monolayer OH and O films on the surface. Under certain *E*-pH conditions hydrogen will also form an adsorbed surface phase.

In future work we plan to consider the cohesive energy of Tc and Fe atoms in various considerations, in order to develop an understanding of how the alloys will dissolve under various conditions. The interplay between surface morphology and environmental chemistry will be critical in determining whether events such as dissolution or repassivation will occur, and what are the competing rates for these processes as a function of pH and electrochemical potential. Examination of the Tc–Fe intermetallic compound will also be important as it is expected that binary alloys will contain a mixture of this intermetallic plus some solid-solution phases. Whereas the parent Tc and Fe phases have similar properties, the binary intermetallic may have unique properties, partially due to the significant size-mismatch between the two elements.

Acknowledgments

Drs. Dave Kolman, Gordon Jarvinen, Dave Moore, and Scott Lillard at Los Alamos National Laboratory are acknowledged for helpful discussions and support. We acknowledge the US Department of Energy (DOE), Office of Nuclear Energy for financial support of this research under the Fuel Cycle Research and Development Program. This research used resources of the Oak Ridge Leadership Facility at the Oak Ridge National Laboratory, which is supported by the Office of Science of the US Department of Energy under Contract No. DE-AC05-00OR22725. Institutional Computing Resources at Los Alamos National Laboratory are also acknowledged. The Los Alamos National Laboratory is operated by Los Alamos National Security LLC for the National Nuclear Security Administration of the US Department of Energy under Contract DE-AC52-06NA25396.

References

[1] E. Deltombe, N. de Zoubov, M. Pourbaix, Atlas of Electrochemical Equilibria In Aqueous Solution, NACE, Houston, Texas, 1974.
[2] L. Fast, J.M. Wills, B. Johansson, O. Eriksson, Phys. Rev. B 51 (1995) 17431–17438.
[3] V.L. Moruzzi, J.F. Janak, A.R. Williams, Calculated Electronic Properties of Metals, Pergamon Press, New York, 1978.
[4] V. Zolyomi, J. Kollar, L. Vitos, Phys. Rev. B 78 (2008) 195414.
[5] S.M. Sichkar, V.N. Antonov, Low Temp. Phys. 31 (2005) 449.
[6] F. Poineau, T. Hartmann, P.F. Weck, E. Kim, G.W.C. Silva, G.D. Jarvinen, K.R. Czerwinski, Inorg. Chem. 49 (2010) 1433–1438.
[7] C. Taylor, Chem. Phys. Lett. 469 (2009) 99.
[8] C. Taylor, M. Neurock, J. Scully, J. Electrochem. Soc. 155 (2008) C407–C414.
[9] G.H. Cartledge, J. Electrochem. Soc. 118 (1971) 1752–1758.
[10] H. Okamoto, Binary Alloy Phase Diagrams, second ed., ASM International, Ohio, USA, 1990.
[11] J. Greeley, J.K. Nørskov, Electrochim. Acta 52 (2007) 5829–5836.
[12] C.D. Taylor, R.G. Kelly, M. Neurock, J. Electrochem. Soc. 154 (2007) F217–F221.
[13] P. Hohenberg, W. Kohn, Phys. Rev. 136 (1964) 864B.
[14] W. Kohn, L.J. Sham, Phys. Rev. 140 (1965) A1133.
[15] J.P. Perdew, K. Burke, M. Ernzerhof, Phys. Rev. Lett. 80 (1998) 891.
[16] G. Kresse, J. Hafner, Phys. Rev. B 47 (1993) 558–561.
[17] G. Kresse, D. Joubert, Phys. Rev. B 59 (1999) 1758–1775.
[18] P. Blonski, A. Kiejna, Vacuum 74 (2004) 179.
[19] J.B. Darby, D.J. Lam, L.J. Norton, J.W. Downey, J. Less-Common Met. 4 (1962) 558.
[20] P. Blonski, A. Kiejna, A. Hafner, Surf. Sci. 590 (2005) 88.
[21] J. Rossmeisl, J.K. Nørskov, C.D. Taylor, M. Neurock, in preparation, J. Phys. Chem. B 110 (2006) 21833.
[22] R.D. Johnson III, NIST Computational Chemistry Comparison and Benchmark Database, NIST Standard Reference Database Number 101, Release 14, September, 2006 (retrieved 02.09.09).
[23] P.J. Linstrom, W.G. Mallard, NIST Chemistry WebBook, NIST Standard Reference Database Number 69, National Institute of Standards and Technology, Gaithersburg MD, 20899 (retrieved 21.09.09).
[24] V. Maurice, H.-H. Strehblow, P. Marcus, Surf. Sci. 458 (2000) 185–194.
[25] B.J. Cruickshank, D.D. Sneddon, A.A. Gewirth, Surf. Sci. Lett. 281 (1993) 308–314.
[26] G. Niaura, Electrochim. Acta 45 (2000) 3507–3519.
[27] C.D. Taylor, R.G. Kelly, M. Neurock, J. Electrochem. Soc. 153 (2006) E207.
[28] R.C. Newman, Stress-corrosion cracking mechanisms, in: P. Marcus (Ed.), Corrosion Mechanisms in Theory and Practice, Marcel-Dekker, New York, NY, 2002.